AGE-ASSOCIATED THIN HAIR DISPLAYS MOLECULAR, STRUCTURAL AND MECHANICAL CHARACTERISTIC CHANGES

F.Baltenneck[1], G.Genty[1], E.BouSamra[1], M.Richena[2], D.P.Harland[2], S.Clerens[2], E.Leccia[3], M.LeBalch[1], R.Betts[4], J.Doucet[3], J-F.Michelet[1], S.Commo[1]

(1) L'Oréal Research and Innovation, Aulnay-sous-Bois, France, (2) AgResearch, Lincoln, New-Zealand, (3) Novitom, Les Ulis, France, (4) 1) L'Oréal Research and Innovation, Singapore, Singapore,

NAME AND DATE OF CONGRESS / Poster ID

1 INTRODUCTION

The thinning of individual hairs occurs during normal chronological aging in women and in men, leading to a changing level of thinner hair shafts alongside original thicker shafts. Progression occurs as an overall hair density decrease in the elderly affecting almost all the individuals and being frequently a source of dissatisfaction for women and men.
Hair shaft forms progressively within a hair follicle during the anagen growing phase of the hair. This process relies on complex molecular interplays between dermal papilla fibroblasts and hair keratinocytes that largely govern both the shape and the diameter of the hair fiber in a given genetic background. So far, the characteristics of age-associated thin hairs remain largely unknown.
The aim of our study was to investigate what is different about the thin hairs that become increasingly prevalent in later life. We therefore compared at multiscale thin and thick hairs from Caucasian women older than 50 years of age. We observed modifications at various levels, namely molecular composition, hair shape, hair fiber organization and mechanical properties.

2 MATERIALS & METHODS

Samples: Hair follicles and scalp biopsies originated from human scalp skin obtained from plastic surgery operations from informed and consenting Caucasian women in the age of 50 to 72 years, living in France. The hair shafts used in this study were taken from the same scalp samples and originated from the the parietal zone (above the ear). Mostly pigmented hairs were collected. Only the proximal end of the shafts (the 20 mm emerging from the scalp) were collected for all tests on hair shafts which ensured that the part of the shaft used in the study was that least affected by consumer interventions

Immuno labelling: Human scalp biopsies from 5 women in the age of 50 to 70 years were cryo-sectioned at 10µm from the hypodermis up to the epidermis. K35 and K38 labeling was carried-out on consecutive sections of pigmented hairs using regular immune-labelling protocols. Guinea pig anti-K35 antibody (1:500) (GP-hHa5, Progen Biotechnik GmbH, Heidelberg, Germany), guinea pig anti-K38 antibody (1:500) (GP-hHa8, Progen, Biotechnik GmbH, Heidelberg, Germany) and the secondary antibody anti-guinea pig Cy3 (1:200) (AP108Cy3, Merck, Darmstadt, Germany) were used. Sections were counterstained with Hoechst (1:5000) for nuclear staining. For the quantitative analyses, pictures were taken at the same distance from the bulb for each hair follicle and image analysis was performed with Image J v. 1.43m software.

Western blotting: Pigmented thin and thick hair shafts from 4 women were cut in small pieces and incubated in an extensive extraction buffer (8 M urea, 2% SDS, 100 mM DTT, 100 mM TrisHCl pH 8,0), vortexed and crushed with a pestle. The supernatants were collected, and the protein concentrations were determined by the Pierce 660 nm method. Western-blots were carried-out with regular protocols with 10 µg of total protein. The primary antibodies GP-hHa5 (anti-K35) or GP-hHa8 (anti-K38) were incubated followed by horseradish peroxidase-labeled secondary antibody. Immuno-blots were revealed using SuperSignal West Dura Extended Duration Substrate (Thermofisher Scientific, Waltham, MA, USA). Peroxidase activity was detected with a CDD camera-based imager. The quantification and normalization were performed with the ImageLab software (Bio-Rad, Hercules, CA, USA). K35 and K38 expression levels were normalized to total proteins content.

Fluorescent Light Microscopy (FLM): Transverse sections of hairs (approximately 2 µm thick), obtained using a histological diamond knife (Diatome Co., Pennsylvania, USA), from 21 subjects (3 thin (diameter < 40µm) and 3 thick (diameter > 70µm) shafts per subject) were stained with fluorescein sodium (FS) solution and 0.0005% sulforhodamine 101 (SR) solution using the method described in Bryson et al. (Bryson et al., 2009). Sections were observed using a DM6000B fluorescence light microscope (Leica Microsystems, Wetzlar, Germany) with I3 filter cube (Excitation filter, band-pass 450-490nm; dichromic mirror 510nm; suppression filter: long-pass 151 nm). Micrographs were taken with a 20x objective. ImageJ FIJI (V1.52R) was used for image analysis.

Transmission Electron Microscopy (TEM): For hair shafts from 8 subjects (one thick and one thin per subject) (sub-set of the 21 subjects used in FLM), comparisons were made on 2 successive sections for each fiber, one of which was treated for fluorescence (double fluorescent staining) and the second stained for TEM observations. Ultrathin sections (100nm thick) were obtained as for FLM, but using a 35° diamond knife (Diatome Co., Pennsylvania, USA). Sections were collected on to Formvar-coated 100 mesh copper grids and stained with uranyl acetate (2%), followed by lead citrate (0.2%). Sections were observed in a Morgagni 268D TEM (Thermofisher Scientific/FEI, Oregon, USA), operating at 80 kV and digital images recorded using a Tengra (Emsis GmbH /Olympus Soft Imaging Systems, Munster, Germany) on-axis camera. TEM-FLM image pairs were used to confirm that, red and green staining in the FLM images correlated with the expected macrofibril structures observed previously (Bryson et al., 2009) and that red corresponded to "low-diameter, high-twist" macrofibrils and green to "high-diameter and low-twist" macrofibrils respectively. TEM observation was then used to compare ultrastrutural differences between thick and thin hairs.

X-ray microdiffraction (µXRD): The preliminary study was carried out at the synchrotron SOLEIL (Saint-Aubin, France). The second set of experiments was made at the European Synchrotron Radiation Facility (Grenoble, France). The two experimental sets were carried out at 23°C and relative hygrometry of about 50%. The diffraction intensity profiles were drawn from patterns obtained in the two angular scattering conditions: WAXS condition, to characterize the low inter-reticular distances (d<10Å) and SAXS condition to characterize the long inter-reticular distances (d>10Å). Comparison of intensities extracted from the diffraction diagrams were made after normalization to consider the volume of matter crossed by the incident beam by subtracting the background signal (measured at 4.35Å far from all characteristic peaks of the hair fiber). Tests were carried out on a set of 6 subjects and 3 thin and 3 thick hair shafts per subject.

3D geometric and swelling characterization: Geometric measurements were achieved with an optical device that enables a 3-dimensional reconstruction of fiber morphology (Franbourg, et al. 2003). The device was designed in our laboratories with an Image Tracer IT 5000 S/N 135 (Zimmer KG, Rossdorf, Germany) for the optical part. A motorized support allowed to explore the full geometry of the fiber in "dry state" (ambient air). Each fiber was characterized by 24500 µm-spaced sections (i.e., 1.2 cm long); each section was characterized by 24 diameters measured on each half-section (7.5° spacing). For each hair, the constant geometry of the shaft was checked along the explored length, and we determined the mean diameter (DMean) from the 24x24 measured diameters and the mean ellipticity e from the max and min diameters. To study the shaft behavior face to water penetration, the UV cell in which the hair was hanged was filled with water. It was possible to determine the characteristics in "wet state" and then the mean swelling ratio in water Sw. 3D swelling tests were carried out on 60 fibers coming from 7 subjects.

Dynamic Mechanical Analysis: Assays were performed on a dynamic mechanical analyzer DMA8000 Perkin-Elmer™ equipped with a water bath and driven with a software Pyris™. The solicitation was a 20Hz ripple sinusoidal signal. Curves of the elastic modulus E' and the loss-angle δ were determined for each fiber during 10min in ambient air and 10min immersed in de-ionized water.

3 RESULTS & DISCUSSION

Hair thinning is accompanied by an imbalance in hair keratin expressions e.g. K38 vs. K35

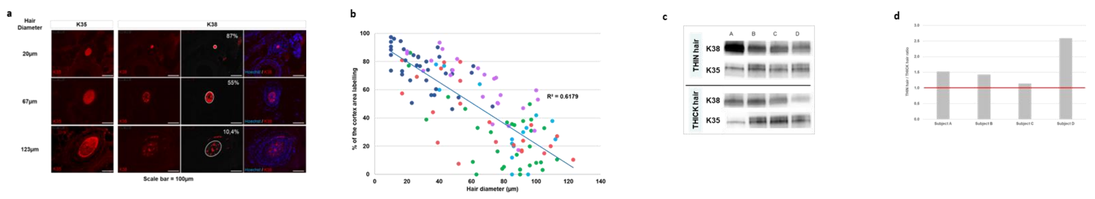

Figure 1 : Immuno-Labelling of K35 and K38 on transversal sections of human thin and thick hair follicles (a, b) and immuno detection of K38 and K35 in hair fiber extracts (c and d).
(a) K35 was labelled in the whole cortex irrespective of hair diameter. By contrast, while K38 labelling highlight the totality of the cortex surface in thin hair, the K38 labelling identified scattered cells in thick hair. (Scale bar = 100 µm). (b) The percentage of K38 labelling in cortex sections of human hair follicle increase when hair diameter decreases; colors represent 5 distinct subjects and linear regression on the whole sample (n: 129 follicles analyzed; R^2 = 0,6179). (c) Immuno blot were quantified, normalized to total proteins. (d) The K38/K35 ratio was increased in thin hair extracts from 3 out 4 subjects (A to D).

Hair thinning is associated with a change of shape, from elliptic to circular

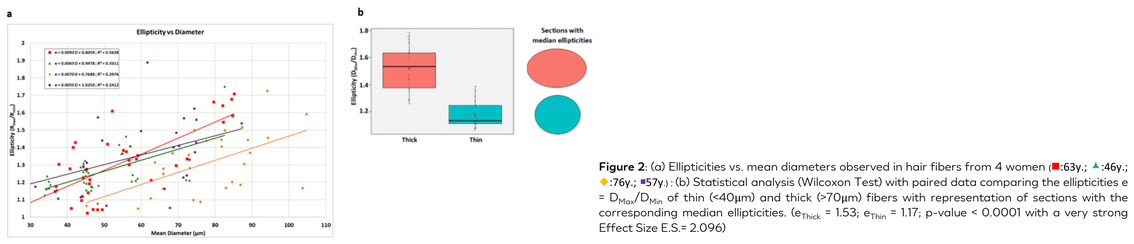

Figure 2: (a) Ellipticities vs. mean diameters observed in hair fibers from 4 women (■:63y.; ▲:46y.; ◆:76y.; ▪57y.): (b) Statistical analysis (Wilcoxon Test) with paired data comparing the ellipticities e = D_{Max}/D_{Min} of thin (<40µm) and thick (>70µm) fibers with representation of sections with the corresponding median ellipticities. (e_{Thick} = 1.53; e_{Thin} = 1.17; p-value < 0.0001 with a very strong Effect Size E.S.= 2.096)

The number of cuticle layers is significantly decreased in thin hairs

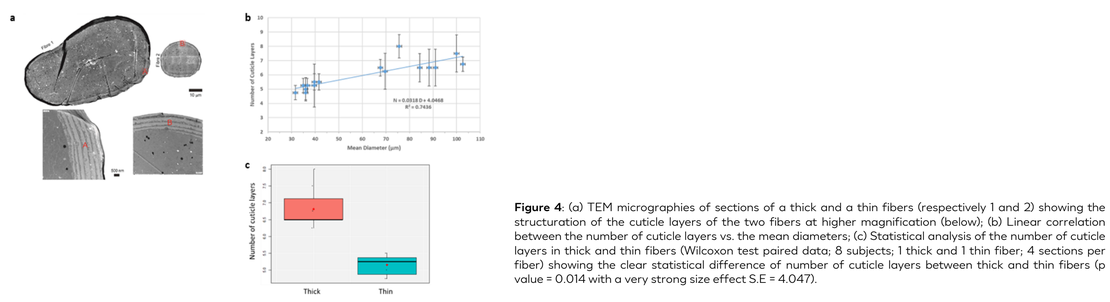

Figure 4: (a) TEM micrographies of sections of a thick and a thin fibers (respectively 1 and 2) showing the structuration of the cuticle layers of the two fibers at higher magnification (below); (b) Linear correlation between the number of cuticle layers vs. the mean diameters; (c) Statistical analysis of the number of cuticle layers in thick and thin fibers (Wilcoxon test paired data; 8 subjects; 1 thick and 1 thin fiber; 4 sections per fiber) showing the clear statistical difference of number of cuticle layers between thick and thin fibers (p value = 0.014 with a very strong size effect S.E = 4.047).

Changes in the expression of hair keratins with hair thinning have consequences on cortex organization

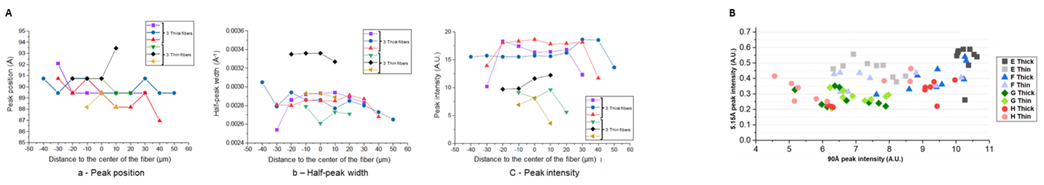

Figure 5: [A] Characteristics of the 90 Å peak (corresponding to the intermediate-filament distance) for thick and thin hair: (a) Peak position; (b) Half-peak width; (c) Peak intensity. Difference between thick and thick fibers are observed on the peak intensity (graph c); [B]: 5.2 Å (a-helix pitch) peak intensity vs 90 Å (intermicrofibrilar distance) peak intensity indicating no correlation between the two parameters.

Thin hairs are stiffer

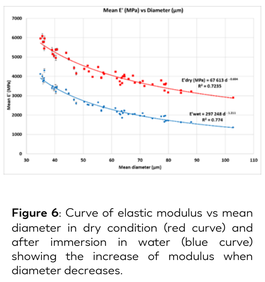

Figure 6: Curve of elastic modulus vs mean diameter in dry condition (red curve) and after immersion in water (blue curve) showing the increase of modulus when diameter decreases.

Viscosity in water decreases in thin hair

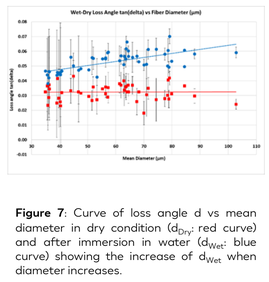

Figure 7: Curve of loss angle d vs mean diameter in dry condition (d_{Dry}: red curve) and after immersion in water (d_{Wet}: blue curve) showing the increase of d_{Wet} when diameter increases.

Penetration of water is slower in thin hair

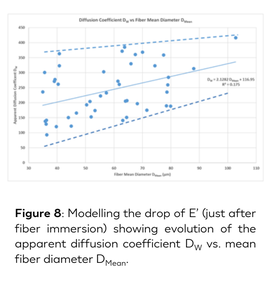

Figure 8: Modelling the drop of E' (just after fiber immersion) showing evolution of the apparent diffusion coefficient D_W vs. mean fiber diameter D_{Mean}.

4 CONCLUSIONS

Age-associated thin hairs exhibit numerous modifications at various levels, namely molecular composition, shape, shaft organization and mechanical properties. These changes did not appear to be linked to the loss of pigment that occurs with age as when white hairs were included in our sample, they did not exhibit different properties. Shape, organization and mechanical properties alterations are likely due to the modifications of hair program as evidenced by the changes in the expression of hair keratins and by the X-ray diffraction specters.

Hence, hair thinning with age does not consist simply of the production of a smaller hair. It is rather a more profound process leading to the production of a hair with new characteristics, likely relying on the implementation of an "aged hair program" that takes place within the hair follicle. Hence, in addition to the inconvenience of leading to a decrease of whole hair volume, hair thinning with age is also responsible for the production of hairs with altered properties.

25th World Congress of Dermatology SINGAPORE 2023

L'ORÉAL RESEARCH & INNOVATION

PLATINUM SPONSOR

REFERENCES

Baltenneck, F., Genty, G., Bou Samra, E., Richena, M., Harland, D. P., Clerens, S., . . . Commo, S. (2022). Age-associated thin hair displays molecular, structural and mechanical characteristic changes. J Struct Biol, 107908. doi:10.1016/j.jsb.2022.107908